A NEW APPROACH TO LEO SPACE DEBRIS SURVEY: THE ITALIAN MULTIBEAM BI-STATIC RADAR 'BIRALES'

Germano Bianchi[(1)], Claudio Bortolotti[(1)], Alessandro Cattani[(1)], Franco Fiocchi[(1)], Andrea Maccaferri[(1)], Andrea Mattana[(1)], Marco Morsiani[(1)], Giovanni Naldi[(1)], Federico Perini[(1)], Alessandra Porfido[(1)], Giuseppe Pupillo[(1)], Mauro Roma[(1)], Simone Rusticelli[(1)] Marco Schiaffino[(1)], Enrico Urru[(2)], Pierluigi Di Lizia[(3)], Matteo Losacco[(3)], Mauro Massari[(3)], Josef Borg[(4)], Denis Cutajar[(4)], Alessio Magro[(4)], Marco Reali[(5)], Walter Villadei[(5)]

[(1)] Istituto Nazionale di Astrofisica - Istituto di Radioastronomia, Via P. Gobetti 101 - 40129 Bologna, Italy, +39 051 6965827, g.bianchi@ira.inaf.it,
[(4)] Istituto Nazionale di Astrofisica – Osservatorio Astronomico di Cagliari, Via della Scienza 5 - 09047 Selargius (CA), Italy,+39 070 711801, eurru@oa-cagliari.inaf.it
[(3)] Department of Aerospace Science and Technology, Politecnico di Milano, Via G. La Masa 34 - 20156 Milano, Italy, +39 02 23998370 pierluigi.dilizia@polimi.it
[(4)] University of Malta, Msida MSD 2080, Malta, +356 2340 3035 alessio.magro@um.edu.mt
[(5)] Italian Air Force – Air Staff, Viale dell'Università 4 - 00185 Rome, Italy, +39 06 49864330, walter.villadei@aeronautica.difesa.it

Keywords: *SST, bi-static radar, Space debris, Italian monitoring network, LEO, multibeam*

ABSTRACT

The aim of this article is to present the architecture proposed for the bistatic radar BIRALES (BIstatic Radar for LEo Surveys) as an instrument for space debris detection in the framework of the European Space Surveillance and Tracking Support Framework (EUSST). In the following paragraphs, the architecture and the upgrades done so far will be presented, as well as the multibeam technology and system calibration.
Eventually, the orbit determination algorithm both for known and unknown objects is described, along with the numerical simulation.

1. INTRODUCTION

During recent years, space debris has arisen severe issues for space mission security, satellites protection, but also for reentry of potentially dangerous tanks down to the Earth.
In 2015, the European Commission, well aware of the topic criticality, took the commitment to implement an European network of sensors for surveillance and tracking of objects in Earth's orbit by starting a dedicated SST (Space Surveillance and Tracking) framework program.
The SST provisions combine the implementation of a newly developed infrastructure, (including optical telescopes, radars and laser stations) with the use and the upgrading of existing European national sensors and operative centers.
Among the sensor selected for the network, the Italian radar 'BIRALES' (BIstatic RAdar for LEo Survey) has been chosen because of its high sensitivity and its key position at the center of the European area.
In this work the BIRALES architecture is proposed as an instrument for the observation of objects in LEO (Low Earth Orbit) in survey mode.

2. SYSTEM ARCHITECTURE

Ground-based radars provide a powerful tool for the characterization of the orbital debris environment. Indeed, they can irradiate at any time a satellite or space debris in Earth orbit with a radio wave beam, and the scattered wave can be detected by a receiver. The receiver position determines whether the radar is monostatic or bistatic. In the former case, the transmitting and the receiving antenna is the same, conversely in the latter case, the receiving antenna can be located up to several miles away from the transmitting.
In more details, BIRALES is a bistatic radar composed of two distinct antennas, a receiving and a transmitting one with a baseline of about 580 km (see Figure 1).

Figure 1: Tx and Rx location

The transmitting antenna is the Radio Frequency Transmitter (TRF- Figure 2) of the Italian Joint Test Range of Salto di Quirra (PISQ) in Sardinia. It consists of a powerful amplifier able to supply a maximum power of 10 kW in the bandwidth 410-415 MHz. It Is a 7 m dish completely steerable at a maximum speed of 3 deg/sec

and with right hand circular polarization. It is available for operation 24 h/day. Its field of view (FoV) matches almost perfectly the receiving antenna one, with a beam of 6 deg.

Figure 2: Radio Frequency Transmitter (TRF)

The receiving antenna is a portion of the Northern Cross Radio Telescope (Figure 3), which is currently one of the largest UHF-capable antenna in the world, being located at the Medicina Radio Astronomical Station, near Bologna, in Northern Italy.
It is owned by the University of Bologna but managed and operated by the Istituto di Radioastronomia at the Istituto Nazionale di Astrofisica (INAF-IRA). It consists of two perpendicular branches: the East-West (E/W) one is 564 m long and consists of a single cylindrical antenna with a width of 35 m, whereas the North-South (N/S) branch is made of 64 parallel antennas with a length of 23.5 m and width of 7.5 m each.

Figure 3: view of the Medicina Radio Astronomical Station. In the foreground, the Northern Cross array

The portion dedicated for the BIRALES receiving antenna is actually composed of 16 parabolic cylindrical antennas of the N/S branche (see Figure 4). The total collecting area is about 2800 square meters and it allows to detect small objects with sub-metric RCS (Radar Cross Section) at 1000 km of altitude.

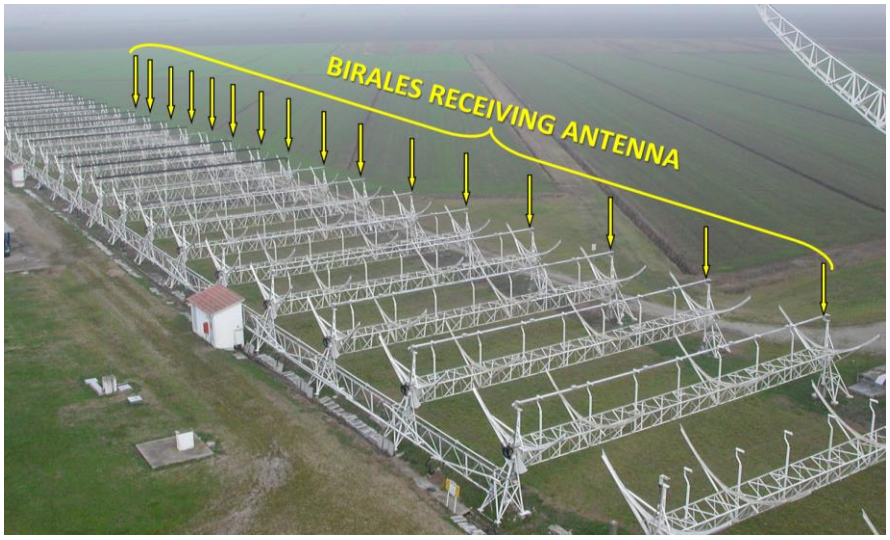

Figure 4: BIRALES receiving antenna

BIRALES works in survey mode and exploits an innovative concept based on multi-beam technique. Indeed, due to the large numbers of receivers installed on the Northern Cross (4 receivers in each N/S antenna for a total of 64 receivers), the Field of View (FoV) can be populated with many independent beams. When an object transits inside the antenna FoV, beams are illuminated by the reflected radio waves. Thus, by looking at the beam illumination sequence, it is possible to estimate the ground track of the transiting objects, with a higher level of details with respect to a single-beam system. The information about the sequence of illuminated beams allows to discern the trajectory of the object with an estimated orbit accuracy below 100 m. The system architecture in shown in the Figure 5.

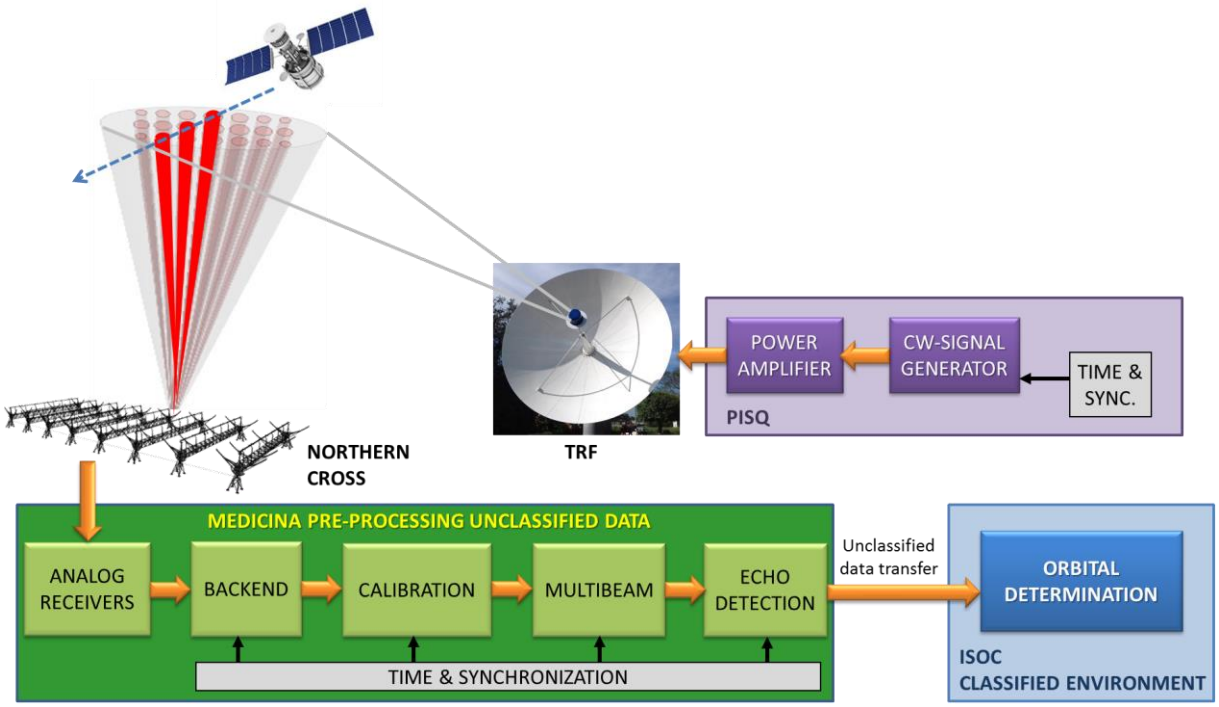

Figure 5: BIRALES system architecture

Using the TRF it is possible to transmit a power CW signal able to illuminate the target in LEO. The echo radio reflected by the orbital object is received through the Northern Cross and the analog signal acquired it is sent to the pre-processing room by an optical fiber link.
The digitized data is processed by means of a data acquisition system based on FPGA boards and CPUs, which digitally assembles measured radar echoes using an FFT in spatial domain in order to calculate the signal present in each beam. Therefore doppler shift, illumination time, antenna pointing angles and measured power intensity (SNR) associated to each beam will be available as well and they are sent to the ISOC (Italian SST Operation Centre) to estimate the orbital of the object detected in a classified environment.

3. ANALOG RECEIVER

The radio echo received by the Northern Cross is amplified by a front-end board installed on the antenna focal line. The box contains also one electro-optical converter which transmits the analog signal to the pre-processing room by the optical fiber link (Figure 6).

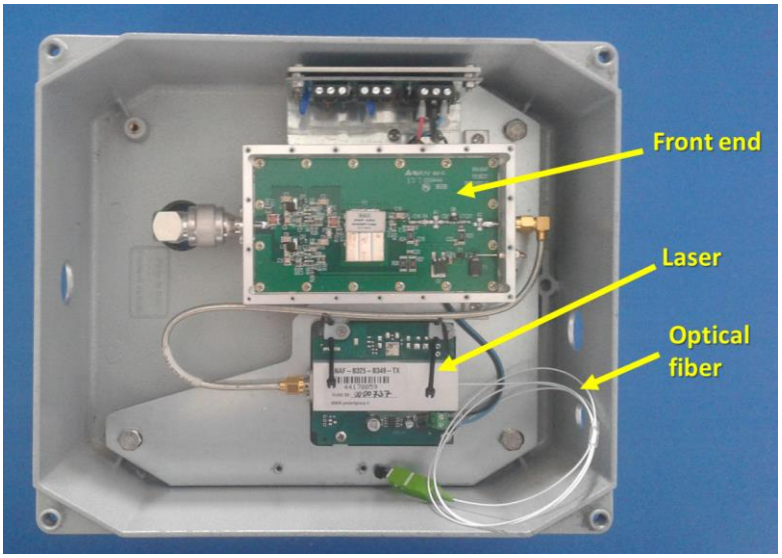

Figure 6: Box installed on the N/S focal line

The front-end performances are:

- NF = 0.45 dB, Tn = 32 K
- Gain = 60 dB
- BW = 16 MHz@408 MHz
- OIP3 > +33 dBm
- InputRL > 15 dB
- OutputRL > 15 dB
- PowerSupply = (10 − 15) Volt @ 245 mA

The optical link is composed of a laser and an optical receiver and its performance was measured in laboratory, putting 500 m of single mode optical fiber between the optical transmitter and receiver (Figure 7).

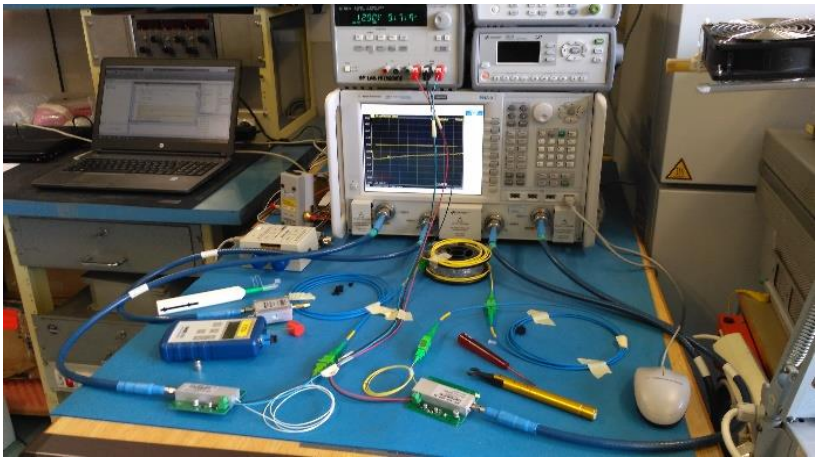

Figure 7: Optical link test bench

The parameters measured for 64 optical link (@400 MHz) were:

- |S11| < -16 dB
- |S22| < -17 dB
- Gain typ = 2 dB ±1
- Noise figure < 35 dB
- OIP3 > 35 dBm
- OIP2 > 47 dBm

The result of the measures are reported in Figure 8.

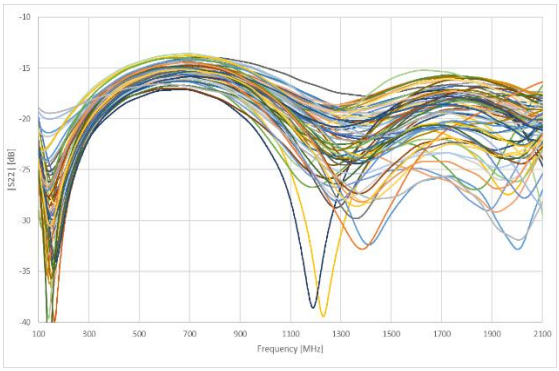

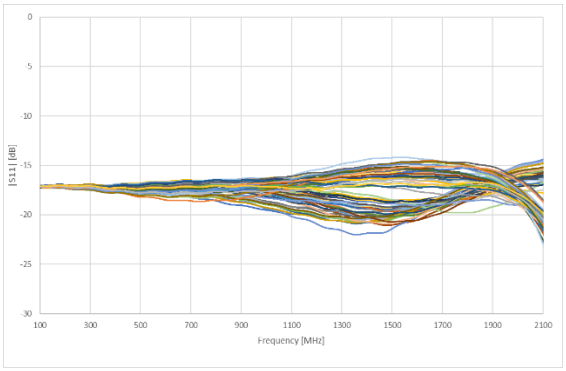

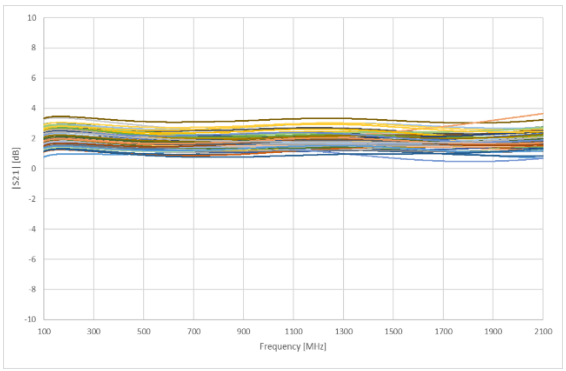

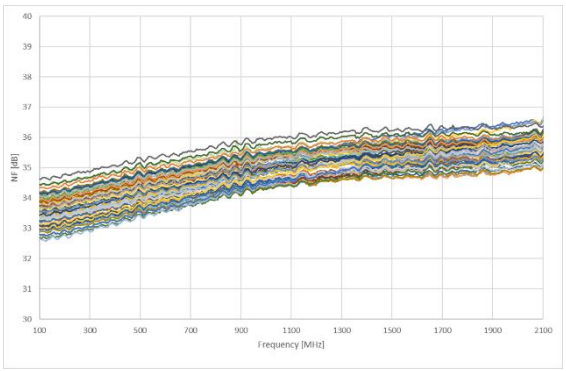

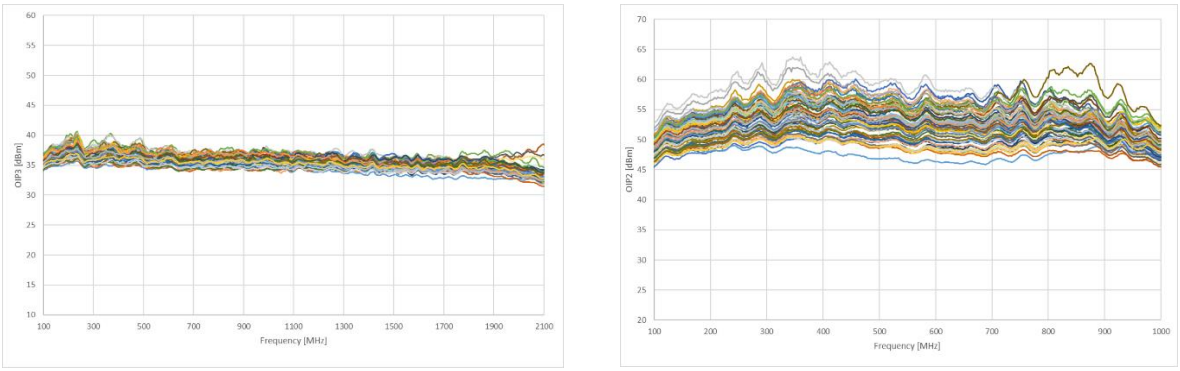

Figure 8: Measure of the optical link parameters

Figure 9 shows some photos taken during the installation of the box containing the front end and optical transmitter. It is possible to see also the installation of the optical fiber and other upgrading phases of the Northern Cross that have been financed by the European Commission thought the H2020 - 3SST2015 program.

Figure 9: Upgrade of the Northern Cross antenna

4. BACKEND

The backend system acquire 64 analog signals coming from 64 antenna receivers and they have to be digitized by 64 ADCs. The analog band at the ADCs inputs is 16 MHz centered at 30 MHz (down converted frequency). The data sampled are sent to a first FFT block in order to generate channels with a sample resolution of 78 KHz, that is the maximum space debris Doppler shift.

The BIRALES system requires a real-time processing backend which can perform fine channelization of the incoming antenna voltages, pixelate the FoV with multiple coherent beams and process each of these beams for detection of debris echoes. Accurate beam pointing requires that the array of antennas will be calibrated. Additionally, the system should be capable of storing and visualizing the results, as well as transmitting them to the orbit determination system. In order to accommodate all these processing stages whilst enabling the addition of new stages with ease, a framework for generating processing pipelines was developed for BIRALES.

The pipelining framework makes up the real-time software back-end. This framework allows for the chaining of different software modules into pipelines, the main ones being:

- The real-time processing pipeline, which receives data from the digital back-end, performs beamforming and channelisation and either writes the resulting data to file or forwards it to the online detection modules for debris detection
- The calibration pipeline, which receives data from the digital back-end and correlates the antenna signals together to generate correlation matrices. These are then used by the calibration routine to generate calibration coefficients to compensate for instrumental phase and gain errors.

5. MULTIBEAM

The multi-beam pipeline performs fine channelization and multi-beaming, such that multiple beams within the array's primary field of view are generated. The resultant beams are then processed by the detection module, which searches for space debris echoes. This pipeline is composed of the following software modules:

Receiver: The digital backend transmits data to the software backend over a 10Gb link, containing a single ~78kHz coarse channel from the 64 antennas. They are transmitted in 32+32 complex fixed point format, which need to be translated to floating point format. The AAVS DAQ library was extended to accept the BIRALES data format and encapsulated as a module. This will read incoming data in chunks and forward the data to the next processing module.

Channelizer: The channel bandwidth is too wide for debris detection, so finer channelization is required. This module implement a polyphase filter bank channelizer, splitting the channel into 8192 ~9.5Hz separate channels, allowing for a temporal resolution of ~10 samples per second. The number of taps is configurable (more taps require more processing), and each antenna is processed by several threads in a thread pool.

Beamformer: The beamformer generates the multi-pixel, which fills the primary field of view with coherent beams, allowing the tracing of debris through the beam. The beam pointing coefficients are static since no tracking is required and the beam

configuration does not change during an observation. The number of beams to generate and where they point within the primary beam are configurable.

6. ECHO DETECTION

The final stage of the BIRALES space debris pipeline is the data detection module. The aim of this data detection module is to analyze the beamformed data outputted by the beamformer module and identify and extract potential space debris candidates. These candidates are persisted into a database to be later retrieved by the orbit determination block. The main stages of the detection module is illustrated in Figure 10 and described in detail in the following sections.

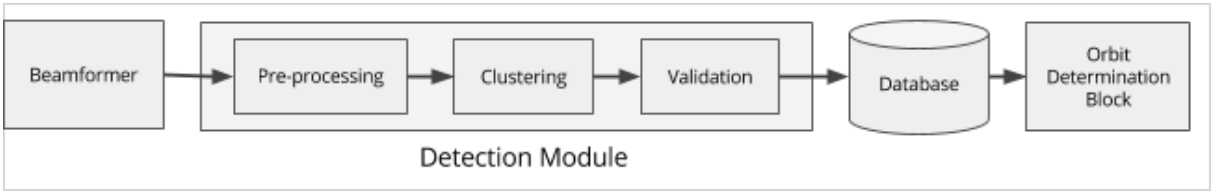

Figure 10: The main stages of the BIRALES Data Detection Module

Pre-processing

The beamformed data, which is encoded as complex voltages, is converted into signal-to-noise ratio (SNR) values. An estimate for the background noise value of the system is calculated by taking the average power value of half of the frequency band for a number of samples before the transmitter is initialized. This is then used as the new estimate for the noise.

This input data is subsequently passed through a number of filters. The aim of the filters is to reduce the number of data points that the detection algorithm has to process. In the first filter, the background noise present is filtered out by considering data points that are two standard deviations away from the mean as being noise. This effectively removes the bulk of the data given that most of the data being processed is noise.

Secondly, the artefacts introduced by the transmitter are removed by applying a transmission line filter, which applies a threshold on those channels in which a time-independent high SNR is recorded. This ensures that the transmission frequency is not considered by the detection algorithm.

The resultant data could still be noisy. This data is usually characterized by random isolated clusters of data points with a low SNR. In order to remove these data points, and reduce the data set even further, a pepper noise filter is applied. The pepper noise filter removes pixels of data which do not have any neighboring pixels.

Clustering algorithm

The DBSCAN clustering algorithm is used to cluster data points together. It is an unsupervised clustering algorithm that works by grouping points that are closely packed together, expanding clusters in any direction where there are nearby points. This way, it is able to deal with different shapes of clusters. Furthermore, it is robust to noisy data, making it an ideal clustering algorithm to be used for this application.

The algorithm is applied to each beam data separately in parallel. The clusters identified by this algorithm are then determined to be potential beam candidates.

Validation of the Beam Candidates

The beam candidates are then validated by a number of criteria. The shape of the space debris detection cluster is expected to be linear. Thus, the next stage of the detection module is to identify 'linear clusters'. The algorithm looks for clusters with a high degree of correlation between frequency and time. In order to do so, the Random sample consensus (RANSAC) regression algorithm was used.

RANSAC, gives a smaller weight to outlier data points, meaning that these data points are ignored. Furthermore, data points that are highlighted as being outliers are removed by the detection algorithm. This means that we not only end up with higher quality clusters (linear clusters with no noise) but it also means that clusters that were eliminated previously because of that one data point are no longer deleted. Another optimization that was introduced was to ignore clusters with an unrealistic doppler shift value.

The remaining validated clusters are then pushed to the space debris queue. The space debris queue is a data structure which was built to hold the validated space debris clusters being identified by the detection algorithm. This data structure ensures that data from the same space debris target is merged into a single space debris object. When the state of the queue changes (by addition or deletion), the space debris candidates are persisted to the database. Candidates that were not modified are not saved again. Once that the candidates are persisted to the database, the user is able to visualize the view the detections through the monitoring application in real-time. In addition, the system is designed such that the detection data can be used by orbit determination routines.

7. CALIBRATION

Both geometric and inherent instrumental delays will interfere with the true sky visibilities, rendering the visibilities measured by the respective antennas out of phase. This directly results in a reduced SNR as a result of destructive interference occurring in the out of phase fringe patterns obtained from correlating the respective antenna visibilities.

While the geometric delays as a result of the position of the antennas in the field in relation to the position of the radio source measured can be easily derived, the same cannot be said for the inherent instrumental delays which might change as a result of a number of factors. Because of the unpredictability and changing nature of such instrumental delays, a simple but robust instrumental calibration is essential for diminishing the resultant lowered sensitivity of an otherwise uncalibrated array. The solution proposed here for the BIRALES receiving array aims to allow calibration to be carried out on a strong point source of relatively stable flux emission in order to characterize instrumental delays. The BIRALES array antennas can only be slewed in altitude, meaning that observation of potential calibration sources can be achieved by slewing to the source’s declination and waiting for the target to transit. The observation would thus be carried out at the time where the source’s RA is equivalent to the local sidereal time.

For this reason, the observed incoming visibilities as a source begins transiting the primary beam are expected to change according to the position of the source in the beam itself, as there is no sidereal tracking undergone. Due both to geometric and instrumental effects, the expected clean bell-shaped peak of the transit visibilities of a strong point source are not however achieved, as the incoming visibilities are out of phase as aforementioned. However, it is known that for a given transit of such a source across the field of view, phase differences between the visibilities of the antennas should be zero when the source is exactly in the beam's zenith, that is, exactly when the source is halfway through the transit.

Stage 1: Peak Source Transit Time Determination

After an observation of a strong source transit, a peak power search is carried out in the correlated visibilities to identify the peak transit of the source through the instrument's beam zenith. The recorded visibilities from all the antennas at each time interval are investigated, in order to determine the time interval at which peak power for the entire transit was measured.

Stage 2: Peak Visibilities Calibration

The array visibilities measured at the peak transit time can thus be identified. Subsequently, per-baseline coefficients are obtained for peak visibilities, which give the expected equal gain and phase values for all visibilities at peak transit. The per-antenna coefficients are then obtained by assuming a reference antenna with zero calibration requirements, and obtaining calibration coefficients for all other antennas with respect to it.

Using per-baseline coefficients obtained for baselines subtended by all other antennas with the reference antenna chosen, this allows for the derivation of calibration coefficients for all the antennas with respect to the reference. In order to eliminate possible anomalous antennas interfering with the calibration procedure, any antennas for which coefficients vary beyond a threshold from the rest of the coefficients are left uncalibrated. The calibration coefficients obtained at this stage, however, incorporate corrections for both instrumental and geometric effects, the latter making them only valid for the declination pointing of the calibrator source in question.

Stage 3: Geometric Effects Subtraction and Subsequent Addition

The final stage in obtaining the instrumental calibration coefficients involves the separation of geometric effects by subtracting geometric corrections from the calibration coefficients obtained, which are a direct result of the position of the source in the sky. After their removal, the resulting coefficients represent the true corrections required to counter inherent instrumental effects only. These coefficients are then fed back to the real-time processing pipeline, such that the resulting beams are well calibrated.

8. ORBIT DETERMINATION ALGORITHM

This section illustrates the orbit determination algorithm. The cases of known and unknown object are studied, and the differences in the implementations are highlighted.

Known Objects

The case of known object refers to the OD process performed on an object whose TLE is available to the user. In this situation, the orbit determination process is divided in two phases. In the first phase, the topocentric deviation of the right ascension and declination, $\Delta\alpha$ and $\Delta\delta$, of the Resident Space Object (RSO) with respect to the receiver nominal pointing direction are evaluated starting from measured SNR and slant range profiles. Then, the object position and velocity vectors are estimated by solving a nonlinear least squares problem.
The evaluation of $\Delta\alpha$ and $\Delta\delta$ profiles is carried out by assuming that the track of the object inside the FoV of the sensor can be approximated with quadratic functions in time. Thus, the time history of the two variables can be expressed as:

$$\begin{cases} \Delta\alpha = a_2 t^2 + a_1 t + a_0 \\ \Delta\delta = b_2 t^2 + b_1 t + b_0 \end{cases} \qquad (1)$$

where *t* is the time elapsed from the starting epoch of observation of the object inside the FoV of the sensor. The estimation of the parameters is divided in two steps (referred to as S1 and S2 in the followings). In S1, the knowledge of the level of measured SNR for each beam and the TLE of the observed object are combined. The procedure goes through the following steps:

- **S1-1.** For each illuminated beam, identify the time instant of maximum illumination, the related SNR, and the topocentric right ascension and declination of the center of the beam.
- **S1-2.** Perform a curve fit that minimizes the angular displacement from each beam center at the time of the maximum received power, selecting as weights the values of the SNR normalized with respect to the maximum SNR among all beams.
- **S1-3.** Evaluate the topocentric $\Delta\alpha$ and $\Delta\delta$ profiles that would be obtained starting from the knowledge of the TLE of the observed object and approximating the real dynamics with the analytical SGP4 model.
- **S1-4.** Rotate the solution obtained by the curve fit along the direction provided by steps S1-3.

The solution obtained with step S1 provides a rough estimation of the right ascension-declination profiles inside the receiver FoV. In step S2, the solution is refined with a nonlinear least square aimed at minimizing the residuals between the measured SNRs and their estimates, obtained with the $\Delta\alpha(t)$ and $\Delta\delta(t)$ guesses. Figures 1a and 1b show the results of the presented algorithms for the case of the object with NORAD ID 27421, according to data reported in Section 2. Beams are colored in grey scale according to the peak SNR measured during the passage (white corresponds to the largest measured SNR). The blue line represents the output of process S1, i.e. the approximated first guess, the red line represents the

computed $\Delta\alpha(t)$-$\Delta\delta(t)$, while the black line is the true trajectory of the object inside the receiver FoV.
Once the topocentric right ascension and declination profiles are obtained, the OD process starts. The aim of the process is to estimate the state of the object at the epoch of the first measurement and it consists of a nonlinear least square optimization to match the orbital trajectory with the range measurements, the Doppler shift data and the right ascension and declination time profiles previously computed. The algorithm starts from an initial guess generated from the TLE and provides at convergence the estimated state vector at the epoch of the first observation and the related covariance matrix.

Unknown Objects

The case of unknown object refers to the OD process performed on an object whose TLE is not available to the user. The algorithm described in the previous section is slightly modified in this case. The unavailability of the TLE does not allow to exploit the knowledge of the state vector for both the estimation of the topocentric right ascension and declination profiles of the object, and the generation of the first guess for the orbit determination process. The first issue is solved by reducing the S1 procedure to its first two steps (S1-1 and S1-2): essentially, the first guess for $\Delta\alpha(t)$ and $\Delta\delta(t)$ is generated considering only the available SNR measurements. Moreover, during the S2 procedure, the radar cross section of the object is included in the set of unknowns of the least square fit. For the second issue, the first guess for the orbit determination process is generated assuming a motion on a circular orbit. The first step consists in identifying the beam of maximum illumination during the passage and the corresponding observation epoch t_1. Then, assuming that the object passes right at the center of the beam at t_1, the position vector $\boldsymbol{r}_1$ is determined by identifying on the line of sight of the beam the point of minimum distance from the transmitter line of sight. Then, the second beam of maximum illumination is considered, a circular motion of the object is assumed, and the position vector $\boldsymbol{r}_2$ at epoch t_2 is determined as the one intersecting the beam line of sight with modulus $||r_1||$. The knowledge of the two position vectors $\boldsymbol{r}_1$ and $\boldsymbol{r}_2$ allows to compute the orbital parameters of the assumed circular orbit and eventually the position and velocity vectors of the RSO at the first observation epoch. The accuracy in the determination of the first guess is strictly related to the validity of the approximations made in the process. In particular, the accuracy of the two position vectors $\boldsymbol{r}_1$and $\boldsymbol{r}_2$ drastically decreases as the actual position of the object at t_1 and t_2 moves away from the center of the selected beams, and this is likely to occur when the maximum detected SNR of those beams is low. This is the reason why the two beams with the largest measured SNRs are selected. The same approach is used for highly-elliptical orbits, though the assumption of circular orbit loses its validity. Once the first guess is defined, the OD process is performed including only gravitational effects in the dynamics due to the unavailability of the ballistic coefficient of the object.

9. NUMERICAL SIMULATION

The results of the performed numerical simulations are presented in this section. An observation window of two days is assumed, covering the range May 25-26, 2016.
The characteristics of the transmitter and the receiver in the analyzed configuration are presented in Table 1.

	Latitude	Longitude	Alt.	Diam.	Power
TX	39°45'31''N	9°27'01''E	205m	7m	10 kW
RX	44°31'25''N	11°38'59''E	25m	-	-

Table 1: Transmitter and receiver characteristics

The beam configuration of the receiver is the one shown in Figure 11, with 32 beams in symmetric configuration. The analysis covers both the cases of known and unknown objects, studying the impact of measurement noise on the accuracy of the orbit determination results.

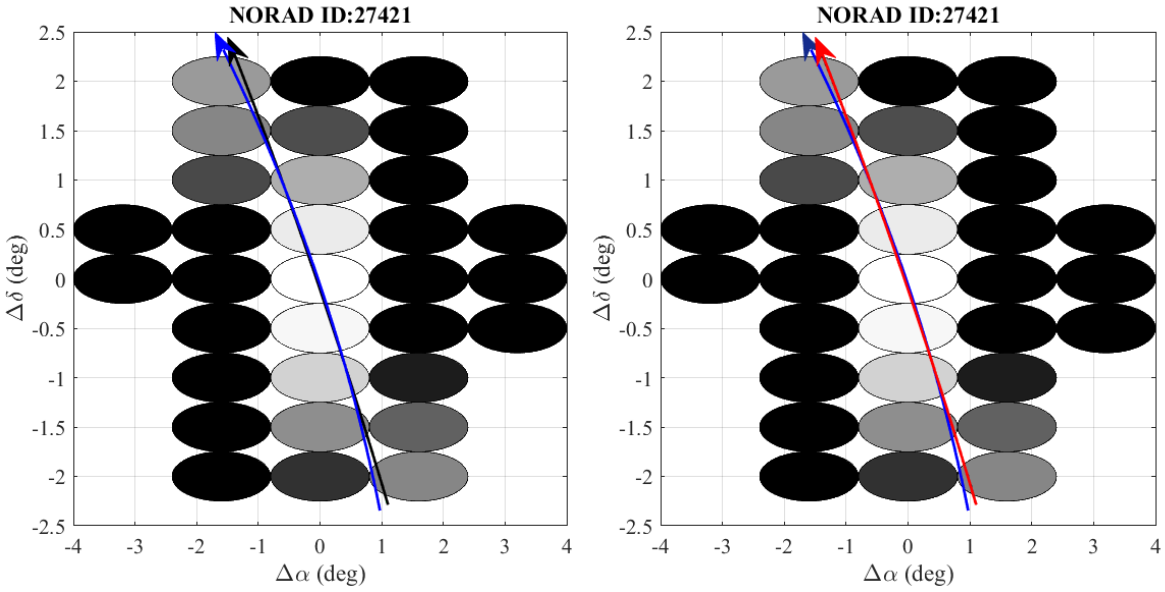

(a). Step S1. First guess identification for $\Delta\alpha$-$\Delta\delta$ (blue line)

(b). Step S2. Time profile refinement (red line)

Figure 11: Right ascension and declination profiles definition inside the receiver FoV for object NORAD ID 27421. The black line represents the real track of the object

Known Objects

The case of known object with no noise measurements represents the first test for the tool.

The number of catalogued objects is 5100, and only 283 can be observed (i.e., have a passage in the FoV of the sensor and generate a detectable SNR level). The reference condition for the error computation is evaluated by propagating the state vector provided by the TLE using AIDA up to the epoch of the first measurement. Table 2, line one, shows the performance of the algorithm in terms of 50th and 75th percentile of the position error in radial direction ($\varepsilon_{p,rad}{}^{50\%}$ and $\varepsilon_{p,rad}{}^{75\%}$), 50th percentile of the position error ($\varepsilon_p{}^{50\%}$) and 50th percentile of the standard deviation in position ($\sigma_p{}^{50\%}$) for the position and, for all the objects with radial error in position lower than 100 m, 50th and 75th percentile of the error in transversal velocity ($\varepsilon_{v,tr}{}^{50\%}\big|_{\varepsilon_{p,rad}<100\ \mathrm{m}}$ and $\varepsilon_{v,tr}{}^{75\%}\big|_{\varepsilon_{p,rad}<100\ \mathrm{m}}$) and 50th percentile of the standard deviation in velocity $\sigma_v{}^{50\%}\big|_{\varepsilon_{p,rad}<100\ \mathrm{m}}$.

	n_{obj}	${\varepsilon_{p,rad}}^{50\%}$	${\varepsilon_{p,rad}}^{75\%}$	${\varepsilon_p}^{50\%}$	${\sigma_p}^{50\%}$	${\varepsilon_{v,tr}}^{50\%}\big\vert_{\varepsilon_{p,rad}<100\text{ m}}$	${\varepsilon_{v,tr}}^{75\%}\big\vert_{\varepsilon_{p,rad}<100\text{ m}}$	${\sigma_v}^{50\%}\big\vert_{\varepsilon_{p,rad}<100\text{ m}}$
No noise	283	0.176 m	0.506 m	0.91 m	0.56 m	0.015 m/s	0.042 m/s	0.04 m/s
Noise in SR and DS	278	1.62 m	3.48 m	6.96 m	101.6 m	1.4 m/s	3.05 m/s	6.6 m/s
Noise in SR, DS and SNR	281	4.13 m	7.96 m	24.5 m	102.5 m	1.4 m/s	3.33 m/s	6.65 m/s

Table 2: Performances of the sensor for the case of known object, standard beam

As can be seen, all errors in position are below 1 m. Moreover, the analysis shows that all objects have a position error in radial direction lower than 100m. The same considerations are valid for errors in velocity, with all terms far below 1 m/s. This trend is quite expected, as the investigated case is the simplest possible, i.e. no disturbances introduced by measurement noise.
The performance of the tool in case of presence of measurement noise is then studied. The first analysis assumes the presence of noise on the slant range (SR) and Doppler shift (DS) measurements. The noise in the slant range is modelled with a Gaussian distribution with zero mean and a standard deviation of 3 m. The Doppler shift noise is modelled by assuming a resolution of 20 Hz. The results are shown in Table 2, second line. As can be seen, the accuracy is worse than in the previous case, though still all objects show a radial error in position lower than 100 m. In particular, position errors increase of one order of magnitude, whereas the decrease in accuracy for the velocity components is more significant. Overall, the influence of the introduced measurement noise is evident, though acceptable.
The measurement noise is finally added to the SNR profiles as a white Gaussian noise, assuming a ratio of 30 dB between the nominal signal and the added white noise. The results of a simulation including all the three contributions to the measurement noise are shown in the third line of Table 2. As can be seen, the combination of all three measurement noises causes a relevant decrease in the accuracy of the results in both position and velocity with respect to the ideal case with no noise, whereas the difference with respect to the case of measurement noise in only SR and DS is less evident.

Unknown Objects

The performance of the sensor in case of unknown objects is now investigated. The inaccuracy in the pointing of the receiver due to the unavailability of the TLE of the object is here modelled as a random error of ±2.5° in the elevation of the receiver with respect to the pointing computed by the simulator.
The results of unknown object and no measurement noise are shown in Table 3, first line. A comparison with the analogous case of known object shows how the error significantly increases when the object is not known a priori. This can be explained with the fact that the unavailability of the TLE in some cases prevents the algorithm from precisely identifying the right ascension and declination profiles of the object, leading to a partially or totally wrong orbit determination. However, the algorithm is still able to perform the orbit determination granting a radial error in position below 100 m for more than the 80% of the cases.

	n_{obj}	${\varepsilon_{p,rad}}^{50\%}$	${\varepsilon_{p,rad}}^{75\%}$	${\varepsilon_p}^{50\%}$	${\sigma_p}^{50\%}$	${\varepsilon_{v,tr}}^{50\%}\big\vert_{\varepsilon_{p,rad}<100\ m}$	${\varepsilon_{v,tr}}^{75\%}\big\vert_{\varepsilon_{p,rad}<100\ m}$	${\sigma_v}^{50\%}\big\vert_{\varepsilon_{p,rad}<100\ m}$
No noise	276	0.64 m	8.9 m	4.18 m	1.2 m	0.032 m/s	0.1 m/s	0.06 m/s
Noise in SR and DS	277	2.66 m	16.2 m	13.3 m	111 m	1.68 m/s	3.76 m/s	6.7 m/s
Noise in SR, DS and SNR	273	8.26 m	46.7 m	49.9 m	111.4 m	1.6 m/s	3.37 m/s	6.7 m/s

Table 3: Performances of the sensor for the case of unknown object, standard beam

The results shown in the second and third lines include the effect of measurement noise. While the introduction of measurement noise on slant range and Doppler shift has a stronger effect on the accuracy in velocity, the combination of all three contributions drastically increases all the errors. The comparison between the two extreme cases of the presented simulations (known objects without measurement noise and unknown objects with all measurement noises) clearly shows how the performance of the algorithm strongly depends on the availability of the TLE of the object and the noise level. Overall, the last case represents, as expected, the most critical scenario.

10. CONCLUSION

BIRALES is a very high sensitivity radar able to detect objects orbiting in LEO in survey mode. Its main characteristics are summarized in the Table 4.

Parameter	Value
Frequency (center band)	408 MHz
Instantaneous bandwidth	16 MHz
Elevation pointing (mechanical)	45° ÷ 135°
Azimuth pointing (electronic)	-3.3 ÷ 3.3 (respect to the meridian)
Instantaneous FoV	30 deg^2 (Dec. 5.7°, RA 6.6°)
Synthetized Beam (pixel)	0.45 deg^2 (Dec 15.5', RA 104')
N of indipendent Beams	48
Minimum detectable RCS	0.02 m^2 @ 750 km

Table 4: BIRALES performances

The minimum detectable RCS of 0.02 m^2 @ 750 km is a conservative number coming from a numerical estimation. In the first test campaign, made on June 2017, we was able to detect smaller objects using only a part of the receiving antenna array. So we have confident to reach a detectable capability of 0.01 m^2.
A Matlab simulation of the pixelated FoV is shown in Figure 12.

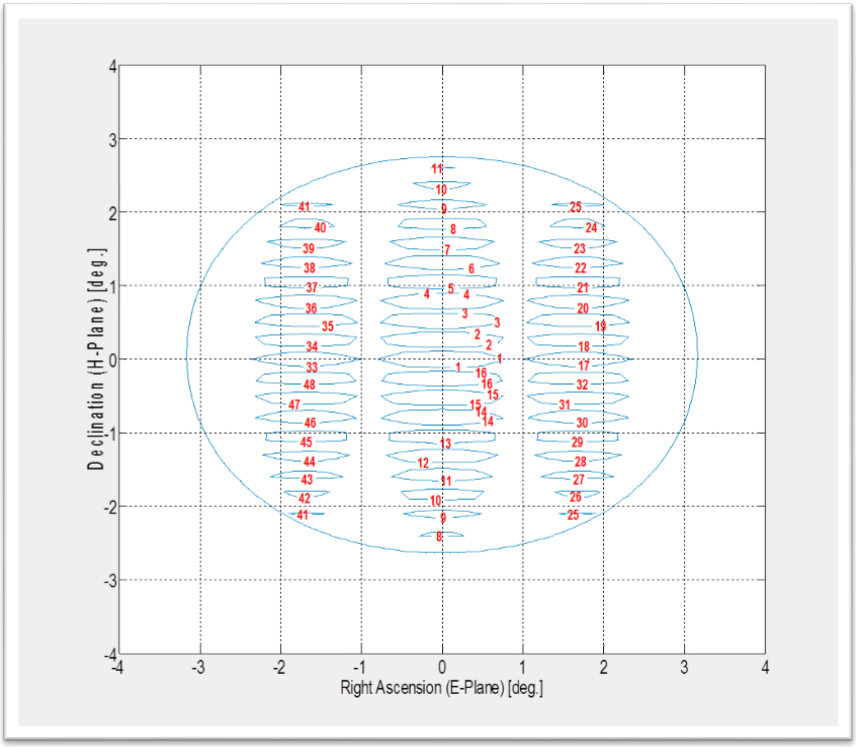

Figure 12: BIRALES pixelated FoV

Regarding the orbit determination, the algorithm proposed is very promising. If the object is unknown, become important to have also an estimation of the range. The ranging measure will be implemented on the system in the next upgrade step.
Hopefully the BIRALES sensor can be operative from December 2017.

11. BIBLIOGRAPHY

[1] Di Lizia P., Massari M., Losacco M., Bianchi G., Mattana A., Pupillo G., Bortolotti C., Roma M., Morselli A., Armellin R., Magro A., Cutajar D., Portelli C., Reali M. "Performance assessment of the multibeam radar sensor BIRALES for SPACE SURVEILLANCE and TRACKING", proceeding of the 7th European Conference on Space Debris, 18-21 April 2017, Darmstadt, Germany.

[2] Morselli A., Di Lizia P., Bianchi G., Bortolotti C., Montebugnoli S, Naldi G., Perini F., Pupillo G., Roma M., Schiaffino M., Mattana A., Salerno E., Magro A., Adami K.Z., Armellin R., Sergiusti A.L., Villadei W., Dolce F., Reali M. "A new high sensitivity radar sensor for space debris detection and accurate orbit determination", proceeding of the 2nd IEEE International Workshop on Metrology for Aerospace, 4-5 June 2015, Benevento, Italy.

[3] Morselli A., Armellin R., Di Lizia P., Bernelli Zazzera F., Salerno E., Bianchi G., Montebugnoli S., Magro A., Adami K.Z., "Orbit Determination of Space Debris Using a Bi-static Radar Configuration with a Multiple-Beam Receiver", In 65th International Astronautical Congress (IAC 2014), 29 September - 3 October, Toronto, Canada, IAC-14-A6.9.4 (2014)

ACKNOWLEDGMENT

The Northern Cross Radio Telescope is a facility of the University of Bologna operated under agreement by the IRA-INAF (Radio Astronomy Institute – National Institute of Astrophysics).

We thank ASI (Italian Space Agency) and ESA (European Space Agency) for the cooperation and the funds in support of this project.

We acknowledge VITROCISET company for providing the transmitting antenna as an in-kind contribution to the project.

We also acknowledge E.S.SAT company for its technical support during the system validation and in particular Daniele Graziani for his expertise.